Hindawi Publishing Corporation
Advances in Materials Science and Engineering
Volume 2014, Article ID 636725, 8 pages
http://dx.doi.org/10.1155/2014/636725

Research Article

Preparation of Aligned ZnO Nanorod Arrays on Sn-Doped ZnO Thin Films by Sonicated Sol-Gel Immersion Fabricated for Dye-Sensitized Solar Cell

I. Saurdi,[1,2] M. H. Mamat,[1] M. F. Malek,[1] and M. Rusop[1,3]

[1] *NANO-ElecTronic Centre, Faculty of Electrical Engineering, Universiti Teknologi MARA, 40450 Shah Alam, Selangor, Malaysia*
[2] *Faculty of Electrical Engineering, UiTM Sarawak, Campus Kota Samarahan, Jalan Meranek, Sarawak, Malaysia*
[3] *NANO-SciTech Centre, Institute of Science, Universiti Teknologi MARA, 40450 Shah Alam, Selangor, Malaysia*

Correspondence should be addressed to I. Saurdi; saurdy788@gmail.com

Received 31 January 2014; Revised 12 June 2014; Accepted 16 June 2014; Published 14 July 2014

Academic Editor: Markku Leskela

Aligned ZnO Nanorod arrays are deposited on the Sn-doped ZnO thin film via sonicated sol-gel immersion method. The structural, optical, and electrical properties of the Sn-doped ZnO thin films were investigated. Results show that the Sn-doped ZnO thin films with small grain size (~20 nm), high average transmittance (96%) in visible region, and good resistivity 7.7×10^2 Ω·cm are obtained for 2 at.% Sn doping concentration. The aligned ZnO nanorod arrays with large surface area were also obtained for 2 at.% Sn-doped ZnO thin film. They were grown on sol-gel derived Sn-doped ZnO thin film, which acts as a seed layer, via sonicated sol-gel immersion method. The grown aligned ZnO nanorod arrays show high transmittance at visible region. The fabricated dye-sensitised solar cell based on the 2.0 at.% Sn-doped ZnO thin film with aligned ZnO nanorod arrays exhibits improved current density, open-circuit voltage, fill factor, and conversion efficiency compared with the undoped ZnO and 1 at.% Sn-doped ZnO thin films.

1. Introduction

One-dimensional ZnO semiconductor has been widely studied because it exists in several advantageous nanostructures, such as nanosheet, nanowires (NWs), and nanoflowers which have attracted much attention for various applications because of their unique properties [1]. Zinc oxide (ZnO) is a wide-bandgap II–VI compound with a 3.37 eV direct bandgap and 60 m eV of free-exciton excitation energy at room temperature. ZnO can be synthesized in many forms of nanostructures via simple and low-cost techniques such as sol-gel and solution-based methods. Various forms of ZnO morphologies and sizes significantly contribute to the novel characteristics of the devices. Many researchers have employed various kinds of ZnO nanostructures [2–4] in dye-sensitized solar cells, which show a significant improvement in the photovoltaic characteristics of the DSSCs. Aligned zinc oxide ZnO nanorod arrays nanostructures provide large surface area and superior carrier transport properties for DSSCs [5, 6]. In addition, the use of a lattice-matched and conducting buffer layer is a feasible way to grow nanorods and NWs, instead of using other materials such as sapphire, that are insulators and expensive. Therefore, the ZnO nanorods and NW arrays grown on metal doped ZnO seed layer are extensively studied. Moreover, Sn-, Al-, Ga-, and In-doped ZnO thin films that show high crystalline structure are useful for practical application on various electronic devices such as solar cells and electroluminescence displays [7–9]. Metal-doped ZnO can be prepared via several techniques such as atomic layer deposition [10], chemical vapour deposition [11], sol- gel [12], pulsed laser deposition [13], RF sputtering [14], spray pyrolysis [15], and so forth. Among these techniques, sol-gel is the most effective in terms of cost and economical production.

In recent years, the ZnO nanorods grown on Al-doped ZnO (AZO) seed layers have been investigated [16, 17].

Yang et al. [18] reported the influence of Sn-doping on ZnO nanorod prepared by hydrothermal method in aqueous solution using zinc nitrate as precursor; however, ZnO nanorods grown on Sn-doped ZnO as seed layers and applied in DSSCs are rarely reported. Moreover, Sn materials, which are originally from group IV elements, exhibit advantages because of their two more extra electrons that can be substituted into ZnO, thereby contributing to double charge carriers. In this study, Sn-doped ZnO films were prepared by sol-gel process. The effects of Sn-doped concentrations on structural, electrical, and optical properties of the as-prepared Sn-doped ZnO thin films were investigated. In addition, the aligned ZnO nanorod arrays were grown on Sn-doped ZnO films using a sonicated sol-gel immersion method. The optical and morphological properties of the aligned ZnO nanorod arrays were also studied. The aligned ZnO nanorod arrays were used as photoanodes in DSSC and their photovoltaic were evaluated.

2. Experimental Detail

The Sn-doped thin films and aligned ZnO nanorods grown on Sn-doped ZnO seed layer were prepared and grown by sonicated sol-gel immersion. Zinc acetate dehydrate (0.4 M, $Zn(CH_3CO_2)_2{\cdot}2H_2O$) was first dissolved in a 2-methoxy-ethanol-monoethanolamine with molar ratio 1 : 1 at ambient conditions. Appropriate amounts of tin doping were doped by adding tin(IV) chloride pentahydrate to the precursor solution. To utilize the Sn-doped ZnO thin films as a seeded layer for ZnO nanorod arrays growth, three solutions with doping concentration Sn/Zn = 0, 1, 2 at.% were prepared. The effects of Sn doping concentration on the structural, optical, and electrical properties of the Sn-doped ZnO thin films and the aligned ZnO nanorod growth at different concentrations (0, 1, and 2 at.%) were investigated in DSSC. The solution was stirred and heated for 3 h before aging for 24 hours at room temperature. The Sn-doped ZnO thin films were spin-coated on glass and ITO substrates at 3000 rpm for 1 min. Each layer of deposited thin film was preheated in air at 150°C to evaporate the solvent. The coating procedure was repeated a few times to increase the film thickness. The thin film was then postheated at 500°C for 1 h in air using an electronic furnace. Corresponding to the different Sn-doped ZnO concentrations (0, 1, and 2 at. %), the obtained thin films were labelled as samples *P*, *Q*, and *R*, respectively. The ZnO nanorod arrays were deposited on Sn-doped ZnO thin film ITO coated glass substrates using zinc acetate solution. The zinc acetate solution was composed of zinc acetate dihydrate, hexamethylenetetramine, and deionized water. The solution was sonicated for 30 min before stirring and aging for 3 h. The ZnO nanorod arrays were grown in water bath at 95°C. The seed layered, ITO-coated glass substrates were immersed into the zinc acetate solution using Schott bottles. The bottles were placed inside the water bath instrument for 1 h for nanorod deposition. After the immersion process, the samples were taken from the bottles and dried in air for 15 min. The samples were annealed in air at 500°C.

To fabricate DSSCs, ZnO nanorod electrode was immersed in 0.5 mM ethanolic solution of $(Ru[LL'(NCS)_2]$, L = 2,2′-bipyridyl-4,4′-dicarboxylic acid, L′ = 2,20-bipyridyl-4,4′-ditetrabutylammonium carboxylate) dye (N719) at room temperature for 24 h. Pt (60 nm thick) sputtered on ITO was used as an electrochemical catalyst for the counter electrode. The substrate with ZnO nanorod electrode and dye was bonded with a sputtered counter electrode using holt-melt spacer. Sealing was accomplished by pressing the two electrodes at approximately 100°C for a few seconds. The electrolytes, composed of 0.5 M Lil, 0.05 M I_2, and 0.5 M 4-*tert*-butyl pyridine (TBP) in acetonitrile, were then introduced into the cell by capillary forces through two holes drilled in the counterelectrode. The holes were covered and sealed to prevent fluid-type electrolyte leakage. The active area of the DSSC device measured using a black mask was 0.25 cm^2. The fabricated DSSC of aligned ZnO nanorod arrays were labelled as samples ZP, ZQ, and ZR. Solar simulator (Bukuh Keiki EP-2000), JASCO UV-VIS/NIR spectrophotometer (V-670 EX), surface profiler (Veeco Dektak 150), X-ray diffractometer (XRD, Rigaku Co., D/MAX-2000), two-probe current-voltage (*I-V*) measurement (Bukuh Keiki EP-2000), field-emission scanning electron microscopic (FESEM, ZEISS Supra 40VP), and energy-dispersive analyser X-ray spectroscope (EDX) were used to characterize the electronic, optical, structural, electrical, and surface properties ZnO nanorod arrays and Sn-doped ZnO thin films.

3. Result and Discussion

Figure 1 shows the FESEM images of the Sn-doped ZnO thin film and the existence of Sn dopant in Sn-doped ZnO thin film was proven by EDX result Figure 1(d). Sn-doped ZnO thin films with flat surface morphology and uniform grain size were prepared by the sol-gel technique. The particle size of the thin film was obviously influenced by the Sn-doped concentration (36, 25, and 20 nm for 0, 1, and 2 at.%, resp.) as estimated in the obtained FESEM images. This phenomenon can be due to substitutional doping, which was attributed to different ionic radii of Sn^{4+} ions and Zn^{2+} ion. Sn^{4+} ion possesses 0.067 nm ionic radius, which is smaller than Zn^{2+} (0.074 nm), thereby retarding the growth process of ZnO crystallization [19, 20] and indicating that the Zn^{2+} is successfully substituted by Sn^{4+} at the lattice point of ZnO [21].

The Sn-doped concentration can also affect the electrical properties of ZnO thin films, in which more electron are produced whenever Sn concentration is increased up to 2 at.%. Two- probe system measurement was employed to study the *I-V* characteristics of ZnO thin films. Figure 2 shows the *I-V* curve of Sn-doped ZnO thin films at −10 V to 10 V applied voltage. All of the prepared thin films show good contact with Au. Furthermore, ZnO thin film doped with 2 at.% Sn shows the highest current intensity among all of the Sn-doped ZnO thin films, reflecting the best optimal electrical properties. By contrast, the undoped ZnO film shows the lowest of current intensity, indicating poor electrical properties. Moreover, the resistivity of the ZnO thin

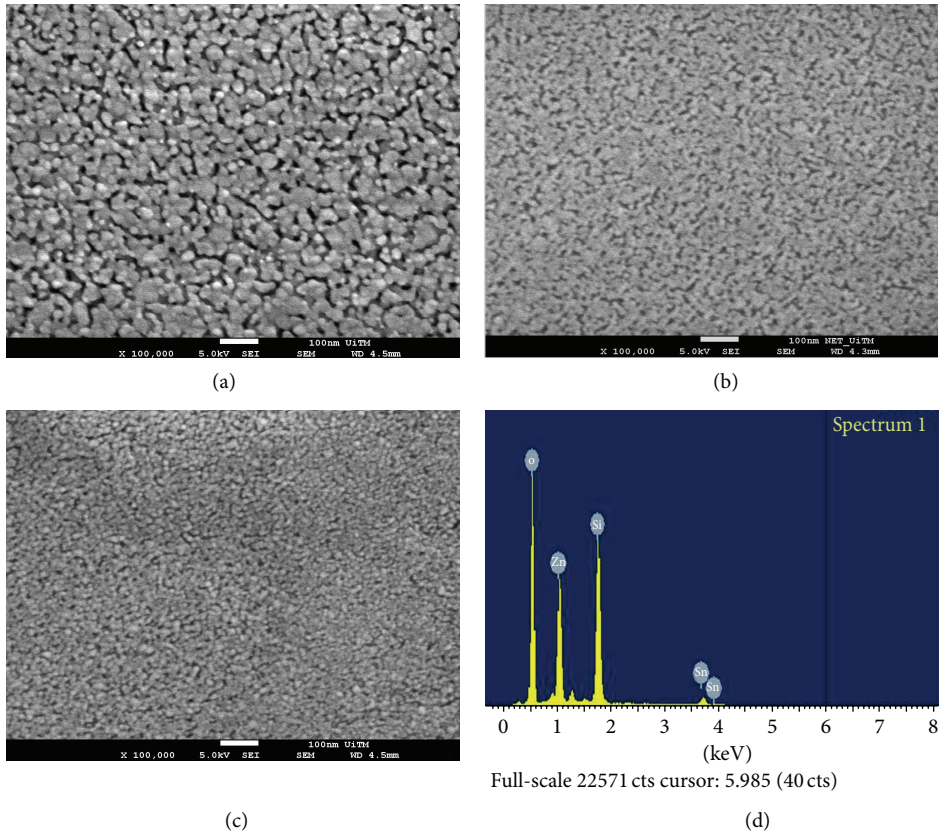

Figure 1: FESEM images of the Sn-doped ZnO films: (a) sample *P*, (b) sample *Q* (c), sample *R*, and (d) EDX at 2 at.% Sn-doped ZnO thin film.

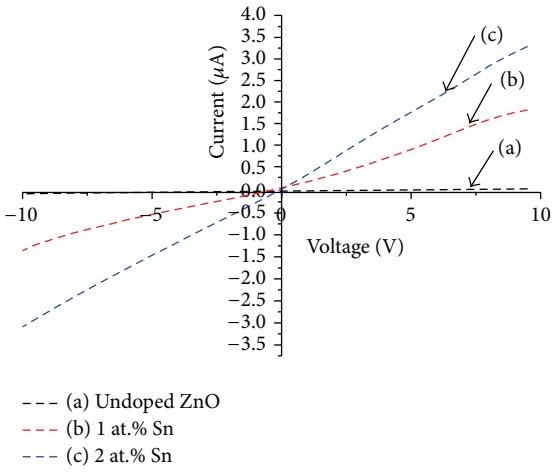

Figure 2: *I-V* curves of the ZnO thin films with different Sn concentrations: (a) sample *P*, 0 at.% Sn, (b) sample *Q*, 1 at.% Sn, and (c) sample *R*, 2 at.% Sn.

films decreases with the increase in doping concentration from 0 at.% to 2 at.% (Figure 2), which also shows the lowest resistivity (7.7×10^2 Ω·cm). Furthermore, the decrease in resistivity of Sn-doped thin film from 0 at.% to 2 at.% was due to substitutional doping of the ZnO structure [22]. Therefore, two free electrons produced from the substitutional doping increased carrier's concentration in the films, which also affect the electron mobility [23]. This result is similar to the one reported by Tsay et al. [24]. In addition, the grain size for sample *Q*-Sn 1 at.% and sample *R*-Sn-2 at.% was smaller than that of the undoped ZnO film. The small grain size can be due to an increment in the transmission line, which is probably caused by the generation of large number of grain boundaries [20].

The transmittance spectra of the ZnO films were measured using UV-Vis-NIR spectrophotometer. As shown in Figure 3(a), all of the thin films exhibit high transparency (>90%) from 400 nm to 800 nm and high absorption edges in the UV region. However, the optical transmittance showed the value of UV region about 65–70%. From the result of EDX in Figure 1(d), there exist four elements which are silicon (18.80%), zinc (16.32%), oxygen (62.93%), and tin (Sn) (1.95%) in atomic percentage. The peak of silicon comes from glass substrate of Sn-doped ZnO films. The ratio of ZnO : O is about 1 : 3.856, whereby the theoretical value of 1 is as expected for ZnO. Therefore, high transparency at UV region might be due to the unreacted zinc along with ZnO films and similar phenomenon has been reported by Shelke et al. [21] and Oh et al. [25]. The transmittance at 2 at.%

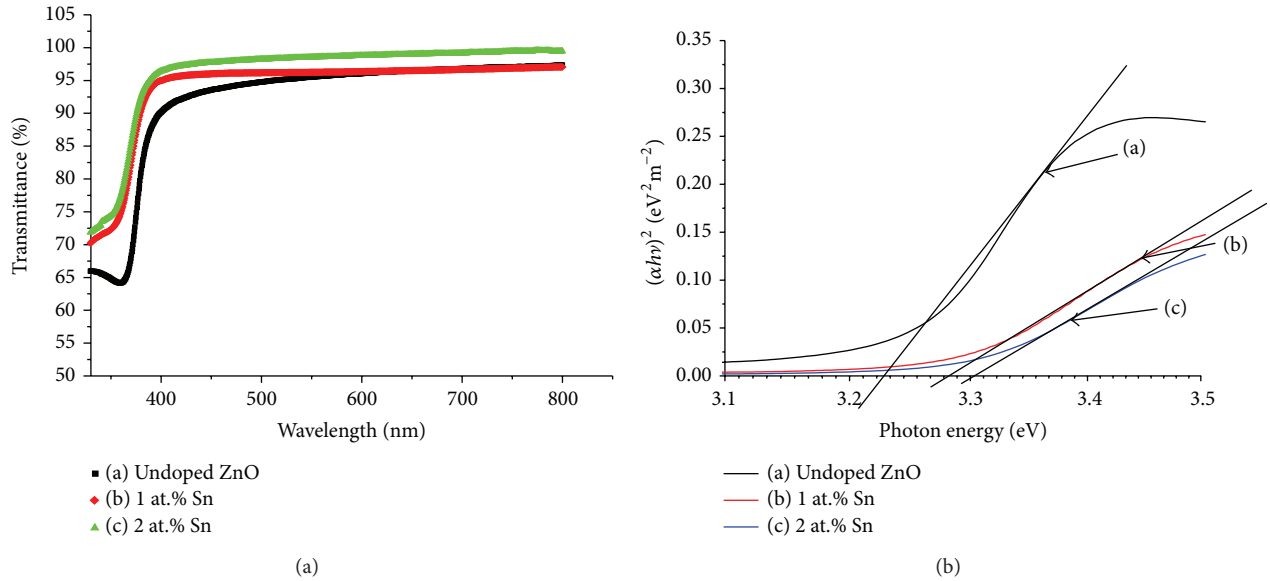

FIGURE 3: (a) Transmittance and (b) optical band gap energy using Tauc's plot.

Sn-doped ZnO thin film exhibited 96% average transparency, which was higher than that of the undoped and 1 at.% Sn-doped ZnO thin film. The high transmittance of thin film can be due to its small surface roughness, thereby suppressing the growth of ZnO Sn dopants and forming flat and fine surfaces [18]. Moreover, the obtained results are comparable with those obtained by Tsay et al. [24] and Pan et al. [26]. High transparency of thin film is useful as window layer in solar cell application. Meanwhile, the optical band gap values of the Sn-doped ZnO were obtained using transmittance data and plotting $(\alpha h\nu)^2$ versus photon energy graphs that also called Tauc's plot. From Tauc's plot in Figure 3(a), the results revealed the band gap of 3.23 eV for undoped which was found to be increased to 3.28 eV and 3.30 after Sn doping 1 at.% and 2 at.%, respectively. Therefore, the thin film tends to blue-shift when the doping concentration increases because of the increase in electron concentration increase and band gap energy broadening. This phenomenon is observed because of the electron with adequate energy supplied from photon energy jumps from the valence band to the conduction band. Therefore, at high Sn concentrations, the Sn-doped ZnO thin film exhibits relatively broadband gap energies compared with those of the undoped ZnO film. Anders et al. [27] reported that the broadening of optical band gap energy can be attributed to Burstein-Moss shift.

Figure 4 shows the surface morphologies of the ZnO nanorod grown on Sn-doped ZnO thin film (0, 1, and 2.0 at.%). The *P*, *Q*, and *R* samples were employed as the seed layer for the growth of the aligned ZnO nanorod. It can be seen that the seed layer with different concentrations of Sn-doped ZnO influenced the morphology and density of the ZnO nanorod arrays. The diameter of the aligned ZnO nanorod grown on sample *R* is smaller than the aligned ZnO nanorod grown on sample *P* and *Q*. This result can be due to the dependence of the diameter of ZnO nanorod and the distances between ZnO nanorods on the grain size and interspaces of the seed layer, respectively, which are confirmed by the results shown in Figure 1 and also similar to the results reported by Zhang and Que [28]. It can be seen that the aligned ZnO nanorods grown on ITO substrate are crystallized along the ZnO [0001] direction, forming hexagonal prisms that are also reported by others [29, 30]. Moreover, the aligned ZnO nanorod grown on sample *R* is the longest among all of the samples. Smaller nanorods and large interspaces between nanorods indicate high surface area as shown in Figures 4 and 5. The nanorod growth is possibly related to the amount of dopants in the ZnO thin films, probably because of high electron concentration in 2 at.% Sn-doped ZnO sample, thereby facilitating the growth of aligned ZnO nanorod arrays [30]. Furthermore, relatively high quantity of the grains is found within the unit area of sample *R* compared with that in samples *P* and *Q* (Figure 1). A larger number of ZnO nanorods are grown on the sample with larger interspaces between ZnO nanorods. In addition, sample *R* smaller grain size leading to smaller ZnO nanorod growth, whereas bigger grain size is observed for samples *P* and *Q* leading to broader ZnO nanorod diameter with denser of ZnO nanorod arrays. The longest ZnO nanorod arrays were found in sample *R*, followed by samples *Q* and *P*. Thus, the larger the grain size the shorter the ZnO nanorod arrays. Based on above results and discussion, the aligned ZnO nanorod grown on sample *R* is suitable for the DSSCs. Moreover, the small nanorods and large interspaces between nanorods are better for dye absorption in DSSC application. The transmittance spectra of ZnO nanorod at different Sn-doped ZnO concentrations (0, 1, and 2 at.%) seeded layer (no N719 and electrolytes) are shown in Figure 6. All of the nanorod exhibit high transparency (50% to 60%) from 400 nm to 800 nm. The regular wave shape of the transmittance suggests that the thickness of ZnO nanorod

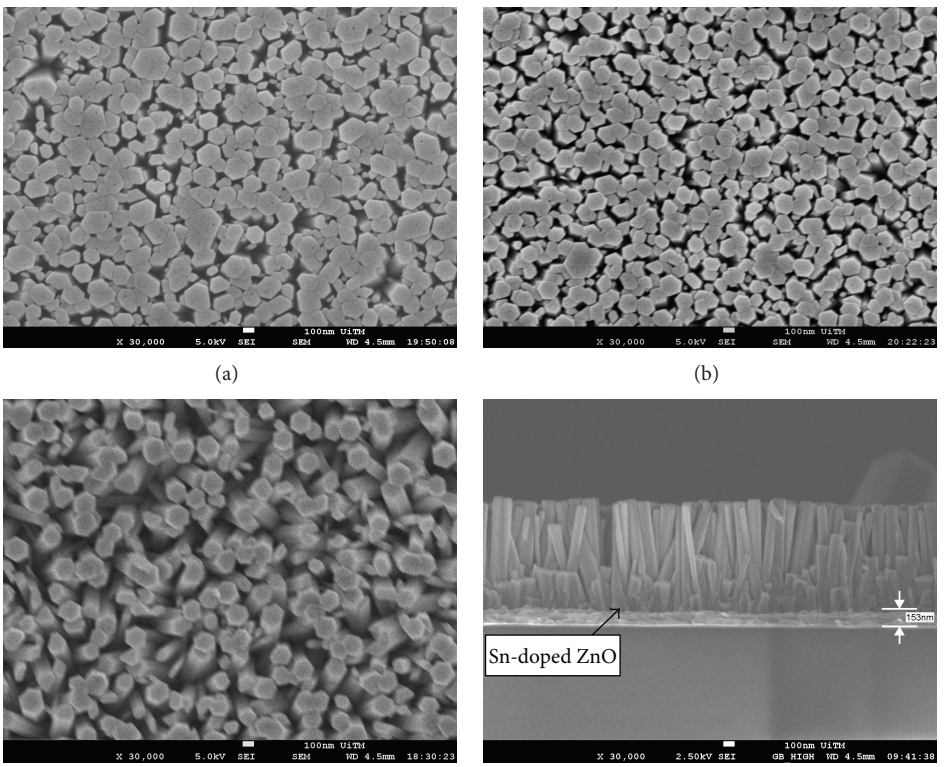

Figure 4: FESEM images of the ZnO nanorods grown on the Sn-doped ZnO seed layer: (a) sample *P*, (b) sample *Q*, and (c) sample *R*. (d) Cross-section of ZnO nanorod sample *R*.

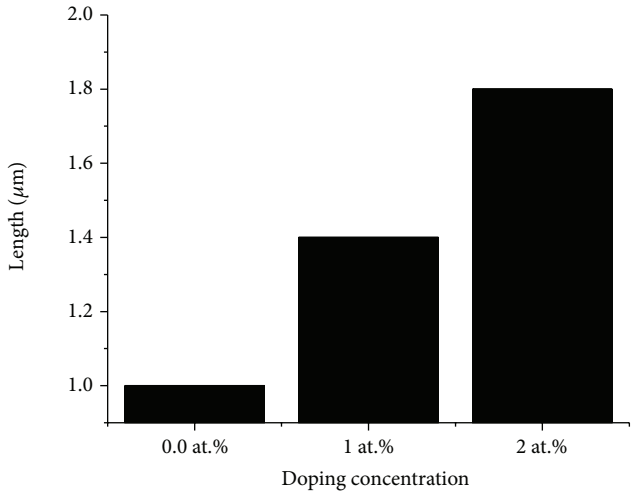

Figure 5: Relationship between the length of the aligned ZnO nanorods arrays and Sn doping concentration.

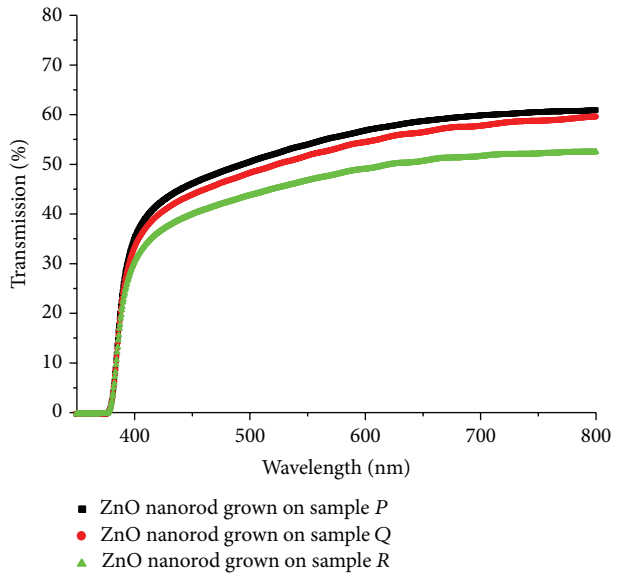

Figure 6: Optical transmittance spectra of the ZnO nanorods grown on samples *P*, *Q*, and *R*.

arrays is uniform, which is also confirmed in Figure 4. The transparency of the ZnO nanorods for samples *P* and *Q* is approximately 60% and 55%, respectively. Meanwhile, the transparency of sample *R* is ~51%, which can be due to surface roughness and verticality of the ZnO nanorod. High surface roughness and poor verticality of the ZnO nanorod can cause high light scattering and decrease transmittance. In DSSCs the dye absorption by the films is one of the main factors in

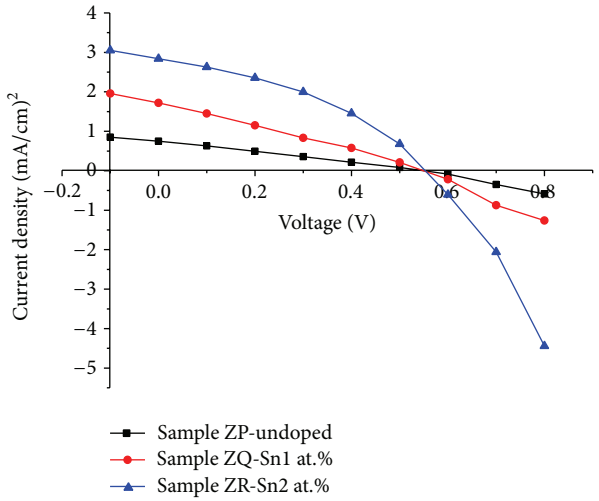

FIGURE 7: I-V characteristics of fabricated DSSCs under light density (100 mW/cm^2).

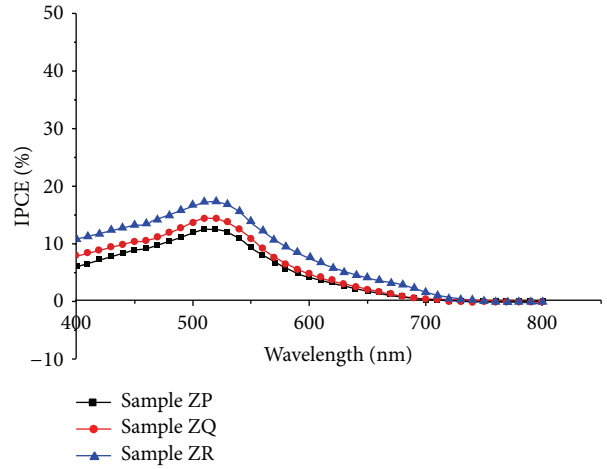

FIGURE 8: IPCE curve of ZnO nanorod DSSC grown on Sn-doped ZnO at different concentrations.

determining the photon energy absorbed from sunlight and transformed as electric current [31–33].

Figure 7 shows the I-V characteristics of the ZnO nanorod DSSC grown at different Sn-doped ZnO concentrations. To investigate the performances of the DSSCs, open-circuit voltage (V_{OC}), short-circuit density (J_{SC}), fill factor (FF), and overall conversion efficiency (η) were calculated as

$$\eta\,(\%) = \frac{(J_{SC}) \times (V_{OC}) \times \mathrm{FF} \times 100}{P_{in}}. \quad (1)$$

The aligned ZnO nanorod photoanode (sample ZR) grown on 2 at.% Sn-doped ZnO film showed higher efficiency than the ZnO nanorod photoanode grown on 1 at.% Sn-doped and undoped ZnO film. Thus, at 2 at.%, the long ZnO nanorods with large surface area are better than P and Q samples. Higher dye absorption in films contributes to the improvement of the photovoltaic properties of the DSSCs. The high density of ZnO nanorod with more pores and large surface can enhance the absorption of photon energy because of high dye absorbed [28, 29]. Meanwhile, high density with less pores and low surface area can cause low dye absorption and thus less photon generation whenever the sunlight illuminates the DSSC. Thus, the photovoltaic properties of ZnO nanorod photoanode on sample ZP (undoped) and sample ZQ (1 at.% Sn) were lower than sample ZR (2 at.% Sn). Table 1 summarizes the photovoltaic performance of the fabricated DSSCs. The J_{sc}, V_{oc}, and energy conversion efficiency η of DSSC of ZnO nanorod photoanode grown at 2 at.% Sn-doped ZnO film were increased. These increases are due to the large surface area of ZnO nanorod, thereby enriching light absorption in high absorption of the N719, which contributes to high photocurrent density. In addition, the multiscattering effect in nanorod can enhance the incident light. The seeded layer of 2 at.% Sn-doped ZnO thin film with low resistivity is also suitable as a buffer layer, in which the recombination between ZnO nanorod as a photoanode and ITO electrode is reduced. Meanwhile, the J_{sc} and V_{oc} for 0 and 1 at.% DSSC with ZnO nanorod are smaller than those of the ZnO nanorod grown on 2 at.% Sn-doped ZnO film. Therefore, the compact structure of ZnO nanorod grown on 0 and 1 at.% films decreases J_{sc} and V_{oc} as well as the performance of DSSCs, which is attributed to less absorption of dye and low photon generation due to high recombination at ZnO nanorod surface. Furthermore, the improvement in current density, fill factor, and conversion efficiency, for ZnO nanorod grown on 2 at.% Sn-doped ZnO film, were increased from 0.749 to 2.84, 0.260 to 0.381, and 0.107% to 0.599%, respectively, compared with those of the ZnO nanorod on undoped film and 1 at.% Sn-doped ZnO film. The improvement in film quality is due to high surface area and high length of ZnO Nanorod grown on 2 at.% Sn-doped ZnO film. This improvement enhanced photovoltaic characteristics of the DSSC.

Figure 8 shows the IPCE of the aligned ZnO nanorod grown on Sn-doped films at different Sn concentrations. The IPCE is the ratio of the number of electrons generated by light in the external circuit to the number of incident photons. As shown in Figure 5, the IPCE of the ZnO nanorod grown at 2 at.% Sn-doped ZnO thin film is approximately 18%. The IPCE of ZnO nanorod grown on 1 and 0 at.% Sn-doped are lower than that of the ZnO nanorods grown on 2 at.% Sn-doped ZnO thin film. With the enhanced ZnO nanorod growth from 0 at.% to 2 at.% Sn-doped film the IPCE values increase from 10% up to 18% at 520 nm. These results confirmed the relatively high current density of the ZnO nanorod grown on sample R. The relatively low IPCE for the two ZnO nanorods (samples P and Q) can be due to high density of ZnO nanorods with less pores and low surface area, which contributed to less dye absorption in the films. Moreover, the relatively high IPCE of ZnO nanorod growth on 2 at.% Sn-doped ZnO film is attributed to the dye absorption caused by high surface area with more pores of film, which consequently increases the incident light intensity in the N719 dye.

Table 1: Photovoltaic performance of ZnO nanorod DSSCs fabricated on different Sn-doped ZnO.

Type of photoanode	J_{sc} (mA/cm^2)	V_{oc} (v)	Fill factor	Efficiency (%)
Sample ZP-0 at.%	0.749	0.548	0.260	0.107
Sample ZQ-1 at.%	1.719	0.549	0.265	0.250
Sample ZR-2 at.%	2.840	0.552	0.381	0.599

4. Conclusion

In this study, the effects of Sn-doped ZnO thin films on the structural, optical, and electronic properties of ZnO nanorod were investigated. The grain size of nanostructured ZnO thin films decreases with the increase in doping concentration. The 2 at.% Sn-doped ZnO thin film shows small grain size, high transmittance, and low resistivity. Moreover, the ZnO nanorods grown on Sn-doped ZnO seed layer exhibit high transmittance in the visible region. Furthermore, the ZnO nanorods grown on 2 at.% Sn-doped ZnO thin film possess large surface area with longer aligned ZnO nanorods. Compared with the undoped film, the improvement of current density, fill factor, and conversion efficiency for ZnO nanorod grown on 2 at.% Sn-doped ZnO film was increased from 0.749 to 2.84, 0.260 to 0.381, and 0.107% to 0.599%, respectively. With the increase in ZnO nanorod growth from 0 to 2 at.% Sn-doped film, the IPCE values increase from 10% to 18% at 520 nm. The improvement in film quality is due to high density, more pores, and long ZnO nanorod grown on 2 at.% Sn-doped ZnO film. These improvements contributed to the enhancement of the photovoltaic properties of the DSSCs. The fabrication of aligned ZnO nanorods grown on Sn-doped ZnO thin film is an important contribution of this study.

Conflict of Interests

The authors declare that there is no conflict of interests regarding the publication of this paper.

Acknowledgments

This work was supported by Grant no. 600-RMI/DANA 5/3/PSI (165/2013) and RAGS/2013/UITM/TK02/1 (600-RMI/RAGS5/3 (52/2013)) from the Ministry of Education Malaysia. The authors would like to thank the Research Management Institute (RMI) UiTM for their support of this research. The authors would also like to thank the NANO-ElecTronic Centre at Faculty of Electrical Engineering and NANO-SciTech Centre at the Institute of Science for the use of their facilities.

References

[1] X. D Wang, J. H. Song, and Z. L. Wang, "Nanowire and nanobelt arrays of zinc oxide from synthesis to properties and to novel devices," *Journal of Materials Chemistery*, vol. 17, pp. 711–720, 2007.

[2] S. Zhu, L. Shan, X. Chen et al., "Hierarchical ZnO architectures consisting of nanorods and nanosheets prepared via a solution route for photovoltaic enhancement in dye-sensitized solar cells," *RSC Advances*, vol. 3, no. 9, pp. 2910–2916, 2013.

[3] M. Law, L. E. Greene, J. C. Johnson, R. Saykally, and P. Yang, "Nanowire dye-sensitized solar cells," *Nature Materials*, vol. 4, no. 6, pp. 455–459, 2005.

[4] Y. Shi, C. Zhu, L. Wang et al., "Optimizing nanosheet-based ZnO hierarchical structure through ultrasonic-assisted precipitation for remarkable photovoltaic enhancement in quasi-solid dye-sensitized solar cells," *Journal of Materials Chemistry*, vol. 22, no. 26, pp. 13097–13103, 2011.

[5] G. K. Mor, K. Shankar, M. Paulose, O. K. Varghese, and C. A. Grimes, "Use of highly-ordered TiO_2 nanotube arrays in dye-sensitized solar cells," *Nano Letters*, vol. 6, no. 2, pp. 215–218, 2006.

[6] M. H. Lai, M. W. Lee, G.-J. Wang, and M. F. Tai, "Photovoltaic performance of new-structure ZnO-nanorod dye-sensitized solar cells," *International Journal of Electrochemical Science*, vol. 6, pp. 2122–2130, 2011.

[7] D. Bao, H. Gu, and A. Kuang, "Sol-gel-derived *c*-axis oriented ZnO thin films," *Thin Solid Films*, vol. 312, no. 1-2, pp. 37–39, 1998.

[8] S. Fujihara, C. Sasaki, and T. Kimura, "Crystallization behavior and origin of c-axis orientation in sol-gel-derived ZnO:Li thin films on glass substrates," *Journal of Applied Surface Science*, vol. 180, no. 3-4, pp. 341–350, 2001.

[9] J. H. Lee, P. Lin, J. C. Ho, and C. C. Lee, "Chemical solution deposition of $Zn_{1-x}Zr_xO$ thin films as active channel layers of thin-film transistors," *Electrochemical and Solid-State Letters*, vol. 9, no. 4, pp. G117–G120, 2006.

[10] S. O. Kucheyev, A. J. Biener, Y. M. Wang et al., "Atomic layer deposition of ZnO on ultralow-density nanoporous silica aerogel monoliths," *Applied Physics Letters*, vol. 86, no. 8, Article ID 083108, 2005.

[11] S. L. Wang, X. Jia, P. Jiang, H. Fang, and W. H. Tang, "Large-scale preparation of chestnut-like ZnO and Zn–ZnO hollow nanostructures by chemical vapor deposition," *Journal of Alloys and Compounds*, vol. 502, no. 1, pp. 118–122, 2003.

[12] V. Shelke, B. K. Sonawane, M. P. Bhole, and D. S. Patil, "Effect of annealing temperature on the optical and electrical properties of aluminum doped ZnO films," *Journal of Non-Crystalline Solids*, vol. 355, no. 14-15, pp. 840–843, 2009.

[13] E. Holemeluad, J. Schou, S. Tauguard, and N. B. Larsen, "Pure and Sn-doped ZnO films by pulsed laser deposition," *Appllied Surface Science*, vol. 197, pp. 467–471, 2002.

[14] N. W. Schmidt, T. S. Totushek, W. A. Kimes, D. R. Callender, and J. R. Doyle, "Effects of substrate temperature and near-substrate plasma density on the properties of dc magnetron sputtered aluminum doped zinc oxide," *Journal of Applied Physics*, vol. 94, no. 9, pp. 5514–5521, 2003.

[15] J. H. Lee and B. Park, "Characteristics of Al-doped ZnO thin films obtained by ultrasonic spray pyrolysis: effects of Al doping and an annealing treatment," *Materials Science and Engineering B*, vol. 106, no. 3, pp. 242–245, 2004.

[16] Y. Nan and C. C. Chun, "Investigation of ZnO nanorods synthesized by a solvothermal method, using Al-doped ZnO seed films," *Optical Materials*, vol. 34, no. 4, pp. 753–756, 2012.

[17] Z. H. Chen, Y. B. Tang, Y. Liu et al., "ZnO nanowire arrays grown on Al: ZnO buffer layers and their enhanced electron field emission," *Journal of Applied Physics*, vol. 106, no. 6, Article ID 064303, 2009.

[18] J. Yang, J. Lee, K. Im, and S. Lim, "Influence of Sn-doping in hydrothermal methods on the optical property of the ZnO nanorods," *Physica E*, vol. 42, no. 1, pp. 51–56, 2009.

[19] J. H. Lee and B. O. Park, "Transparent conducting ZnO:Al, In, thin films deposited by the sol-gel method," *Thin Solid Films*, vol. 426, no. 1-2, pp. 94–99, 2003.

[20] K. J. Chen, F. Y. Hung, Y. T. Chen, S. J. Chang, and Z. S. Hu, "Surface characteristics, optical and electrical properties on sol-gel synthesized sn-doped ZnO thin film," *Materials Transactions*, vol. 51, no. 7, pp. 1340–1345, 2010.

[21] V. Shelke, B. K. Sonawane, M. P. Bhole, and D. S. Patil, "Electrical and optical properties of transparent conducting tin doped ZnO thin films," *Journal of Materials Science: Materials in Electronics*, vol. 23, no. 2, pp. 451–456, 2012.

[22] J. Lee, W. Gaoz, L. M. Hodgson, J. Metson, H. Gong, and U. Pal, "Sputtered deposited nanocrystalline ZnO films: a correlation between electrical, optical and microstructural properties," *Applied Physics A: Materials Science and Processing*, vol. 80, no. 8, pp. 1641–1646, 2005.

[23] S. Venkataraj, S. Hishita, Y. Adachi et al., "Structure and electric properties in tin-doped zinc oxide films synthesized by pulsed laser deposition," *Journal of the Electrochemical Society*, vol. 156, no. 6, pp. H424–H429, 2009.

[24] C.-Y. Tsay, H.-C. Cheng, Y.-T. Tung, W.-H. Tuan, and C.-K. Lin, "Effect of Sn-doped on microstructural and optical properties of ZnO thin films deposited by sol-gel method," *Thin Solid Films*, vol. 517, no. 3, pp. 1032–1036, 2008.

[25] H. Oh, J. Krantz, I. Litzov, T. Stubhan, L. Pinna, and C. J. Brabec, "Comparison of various sol-gel derived metal oxide layers for inverted organic solar cells," *Solar Energy Materials & Solar Cells*, vol. 95, no. 8, pp. 2194–2199, 2011.

[26] Z. Pan, X. Tian, S. Wu et al., "Effects of Al and Sn dopants on the structural and optical properties of ZnO thin films," *Superlattices and Microstructures*, vol. 54, no. 1, pp. 107–117, 2013.

[27] A. Anders, S. H. N. Lim, K. M. Yu et al., "High quality ZnO:Al transparent conducting oxide films synthesized by pulsed filtered cathodic arc deposition," *Thin Solid Films*, vol. 518, no. 12, pp. 3313–3319, 2010.

[28] J. Zhang and W. Que, "Preparation and characterization of solgel Al-doped ZnO thin films and ZnO nanowire arrays grown on Al-doped ZnO seed layer by hydrothermal method," *Solar Energy Materials and Solar Cells*, vol. 94, no. 12, pp. 2181–2186, 2010.

[29] X. Tao, M. Fu, A. Zho, D. He, and Y. S. Wang, "The effect of seed layer on morphology of ZnO nanorod arrays grown by hydrothermal method," *Journal of Alloys and compounds*, vol. 489, no. 1, pp. 99–102, 2010.

[30] H. K. Lee, M. S. Kim, and J. S. Yu, "Effect of AZO seed layer on electrochemical growth and optical properties of ZnO nanorod arrays on ITO glass," *Nanotechnology*, vol. 22, no. 44, Article ID 445602, 2011.

[31] M. Kao, H. Chen, S. Young, C. Lin, and C. Kung, "Structure and photovoltaic properties of Zno nanowire for dye-sensitized solar cells," *Nanoscale Research Letters*, vol. 7, article 260, 2012.

[32] W. Yang, F. Wan, S. Chen, and C. Jiang, "Hydrothermal growth and application of ZnO nanowire films with ZnO and TiO_2 buffer layers in dye-sensitized solar cells," *Nanoscale Research Letters*, vol. 4, pp. 1486–1492, 2009.

[33] Y. F. Gao, M. Nagai, T. C. Chang, and J. J. Shyue, "Solution-derived ZnO nanowire array film as photoelectrode in dye-sensitized solar cells," *Crystal Growth and Design*, vol. 7, no. 12, pp. 2467–2471, 2007.